

5. LOW-TEMPERATURE ALTERATION OF BASALT OVER TIME: A SYNTHESIS OF RESULTS FROM OCEAN DRILLING PROGRAM LEG 187¹

D.J. Miller^{2,3} and J. Kelley²

ABSTRACT

Shipboard studies during Ocean Drilling Program Leg 187 (Australian Antarctic Discordance, AAD) suggested that there was no discernible coincidence between the interpreted age of rocks recovered and the intensity of alteration observed. Samples from the oldest sites occupied appeared to exhibit the least overall effects of alteration, and the intensity of alteration varied from site to site. Previous investigations of low-temperature alteration in oceanic basement samples have been restricted by the myopic perspective provided by single drill holes or dredge collections. Combining core samples from Leg 187 and dredge samples from the AAD collection at Oregon State University (USA) offers the unique opportunity to investigate mineral and bulk chemical changes attending alteration of basalt over a range of ages from 0 to 28 Ma. Results of this research indicate that there is a general increase in the intensity of alteration as the basalts age and move off axis, but that this relationship is somewhat veiled by the dominating control on alteration intensity dictated by variations in permeability.

INTRODUCTION

The primary objective of Ocean Drilling Program (ODP) Leg 187 was to locate the Indian/Pacific mantle isotopic boundary using the geochemistry of mid-ocean-ridge basalt (MORB) lavas erupted over the

¹Miller, D.J., and Kelley, J., 2004. Low-temperature alteration of basalt over time: a synthesis of results from Ocean Drilling Program Leg 187. *In* Pedersen, R.B., Christie, D.M., and Miller, D.J. (Eds.), *Proc. ODP, Sci. Results*, 187, 1–29 [Online]. Available from World Wide Web: <http://www-odp.tamu.edu/publications/187_SR/VOLUME/CHAPTERS/206.PDF>. [Cited YYYY-MM-DD]

²Department of Geology and Geophysics, Texas A&M University, College Station TX 77845, USA.

³Integrated Ocean Drilling Program, Texas A&M University, 1000 Discovery Drive, College Station TX 77845-9547, USA.

miller@iodp.tamu.edu

last 28 m.y. north of the Australia Antarctic Discordance (AAD). This boundary was reasonably well constrained for young basalts (0–5 Ma) by dredging expeditions, but the limited areal extent of the dredging sample suite allowed for several competing hypotheses of long-term mantle boundary geometry defined by either the rate of incursion of one mantle province into the other or by the longevity of the present mantle boundary configuration. Leg 187 set out to sample rocks in the range of 10–30 Ma with a reactive drilling strategy that was expected to eliminate all but one of these competing hypotheses. One unanticipated yet exciting result of this sampling strategy was recovery of a MORB time series produced on the Southeast Indian Ridge that records the effects of low-temperature alteration of the ocean crust over the range from 14 to 28 Ma. These samples, when combined with samples from the aforementioned dredge collection, yield the opportunity to evaluate the magnitude and direction of chemical fluxes associated with low-temperature hydrothermal alteration of ocean crust over nearly 30 m.y.

Whereas the most dramatic evidence of hydrothermal alteration of the ocean crust is associated with high-temperature environments and several ODP legs have been devoted to investigation of these (e.g., Davis, Mottl, Fisher, et al., 1992; Humphris, Herzig, Miller, et al., 1996; Fouquet, Zierenberg, Miller, et al., 1998), significantly greater fluxes of heat and seawater are exchanged at lower temperature. If heat flow observations and models are correct, advective heat loss on ridge flanks is responsible for several times more heat and fluid exchange than occurs in high-temperature, ridge-crest systems (e.g., Davis, Fisher, Firth, et al., 1997). These models suggest that heat loss may continue for several tens of millions of years as the crust moves away from ridge crests (e.g., Anderson et al., 1977; Sclater et al., 1980). One intriguing result of Leg 187, however, is that, based on shipboard observations, there is no apparent coincidence between the age of the crust and the degree of low-temperature hydrothermal alteration. In fact, the initial impression of core describers was that the least-altered basalts were recovered from the oldest crust sampled. Intuitively, this suggests that the effects of alteration are invested at or near the ridge crest and are not significantly modified over time, which may not be consistent with heat flow models.

In addition, recent investigations along the Juan de Fuca Ridge have suggested that different segments of the ridge crest are at different stages of magmatic and tectonic evolution, resulting in differences in the observed hydrothermal activity (e.g., Hammond, 1990; Delaney et al., 1992; Embley and Chadwick, 1994). Alternatively, alteration studies from Hole 504B, off the Costa Rica Rift, suggest permeability variations are the primary control on the intensity of alteration (Alt et al., 1986, 1996). However, all these studies are constrained to samples from either a single or a very few drill holes, dredge rocks, or discontinuous samples (i.e., data from rocks from different ocean basins), which might provide a biased perspective of the long-term, overall nature of low-temperature alteration. A more complete data set, one that includes samples covering a range of ages, coming from strategic locations relative to an active spreading ridge and including a great number of fresh, altered, and glass samples is needed to more accurately assess long-term alteration trends.

Our drilling sampled a transect east of the AAD that is characterized by an axial ridge with smooth off-axis topography similar to fast-spreading crust. We also sampled two transects within the AAD that are

characterized by deep axial valleys with rough off-axis topography akin to slow-spreading crust. These two sets of transects represent lavas that were erupted at 14–28 and 16–25 Ma, respectively. Complementing this suite with samples dredged from near the spreading axis (0–7 Ma) allows us to investigate distinctions in alteration characteristics between these markedly different ridge segments and compare to differences reported from the previous investigations.

The principal objective of this synthesis is to integrate results on various aspects of low-temperature alteration (<350°–400°C) to document the alteration mineral chemistry and bulk chemical alteration characteristics of lavas of various ages from the upper oceanic crust near the AAD and from this to determine the conditions of alteration and any time- and/or location-dependent changes in alteration characteristics in these samples and to assess the direction and magnitude of bulk chemical changes produced by alteration of these basalts.

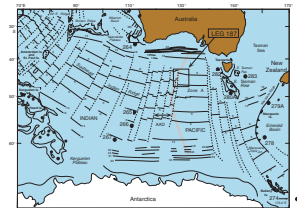
REGIONAL GEOLOGY AND PREVIOUS WORK

The AAD is an anomalously deep region of the Southeast Indian Ridge (SEIR) between ~120° and 127°E (Fig. F1). This region is characterized by chaotic topography, numerous short axial ridge segments with long alternating transform offsets, unusually thin crust, high seismic velocities in the upper mantle, and nonuniform spreading. Two potential causes of these characteristics have been championed: relatively cold upper mantle underlying the AAD and the convergence of two mantle flows in the underlying asthenosphere (Sempéré et al., 1991; Weissel and Hayes, 1971; Forsyth et al., 1987; Palmer et al., 1993; Christie et al., 1998; West et al., 1994; West, 1997; Marks et al., 1990). In the Leg 187 area of operations previous researchers adopted a shorthand terminology to refer to different segments of the SEIR (Fig. F2). Zone A refers to the region east of the AAD, and the easternmost part of the AAD is referred to as Zone B. For ease of discussion and comparison to previous work, this terminology will be used here.

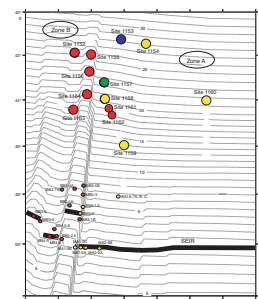
Both zones have an intermediate spreading rate, though morphologically, deep axial valleys with chaotic off-axis topography typical of slow-spreading crust are found in Zone B and high axial ridges with smooth off-axis topography associated with fast-spreading rates are found in Zone A. This morphological change is one boundary located between Zone A and Zone B directly on the SEIR that continues off axis. Another boundary is located in the easternmost region of Zone B. This is an isotopic boundary, marked by differences in Pb, Nd, and Sr contents of lavas, indicative of the convergence of the underlying mantle provinces (Christie, Pederson, Miller, et al., 2001).

During Leg 187, 13 sites near the AAD were sampled (Figs. F1, F2). As a consequence imposed by current drilling technology, all these sites are in isolated, localized (one to a few kilometers across, a few tens to four hundred meters deep) sediment pockets disseminated throughout a region characterized by a thin veneer of sediment resting on topographically rough basement that resists dredging attempts. The shipboard drilling and sampling strategy dictated that only the freshest samples recovered were routinely analyzed on board for major and trace elements. Additionally, most of the thin sections prepared on board were from the same pieces as those sampled for geochemical analysis, so the shipboard data set is biased toward the fresher samples.

F1. Map of the Southeast Indian Ocean, p. 14.



F2. Site locations in relation to seafloor isochrons, p. 15.



METHODS

The focus of this synthesis is to complete characterization of the rocks recovered during Leg 187 by compiling and interpreting data from the abundant altered material recovered. In addition, we include data from samples dredged from on or near the spreading axis collected during two expeditions to the AAD (Moana Wave and Boomerang 5).

Glasses were handpicked and fresh basalt samples were selected for shipboard analysis of major and trace elements. The fresh basalts and glasses were analyzed using inductively coupled plasma-atomic emission spectrophotometer (ICP-AES, shipboard) and X-ray fluorescence and ICP-mass spectrometry (ICP-MS, shore based), and results are reported in the Leg 187 *Initial Reports* volume (Christie, Pedersen, Miller, et al., 2001). Altered basalts were selected on shore for whole-rock analysis of the major, trace, and rare earth elements by ICP-AES and ICP-MS and were conducted by Acme Analytical Laboratories, Vancouver, British Columbia (Canada). Samples chosen were free of glass, veins containing secondary minerals, and any other foreign material. After washing and drying in the oven, the samples were pulverized in an alumina-ceramic shatterbox for 5 min. Duplicate samples as unknowns and U.S. Geological Survey standard reference materials (SRM) were included in each analytical suite to check accuracy and precision.

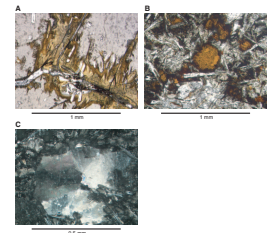
Hand-specimen and thin section observations were used to characterize bulk alteration features. Fracture and vein density statistics were recorded during Leg 187 by the structural geology team (Christie, Pederson, Miller, et al., 2001), and intervals of interest were reexamined during this study. Approximately 45% of the core recovered during Leg 187 consisted of oriented pieces. Some holes (specifically Holes 1155A, 1158A, and 1160A) returned significantly lower numbers of oriented pieces or had exceeding low recovery, so we consider the structural data measured on these cores to be the least representative.

RESULTS

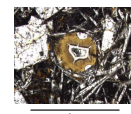
Common primary phases include plagioclase, clinopyroxene, olivine, and minor to trace amounts of iron-titanium oxides and sulfide minerals (Christie, Pedersen, Miller, et al., 2001). Table **T1** is a summary of our petrographic analysis of the altered samples used in this study. Details of fresh samples can be found in the Leg 187 *Initial Reports* volume (Christie, Pederson, Miller, et al., 2001). Secondary minerals are represented almost entirely by Fe oxyhydroxides, clays (smectite group according to X-ray diffraction data), and palagonite, and these products are ubiquitous at every site. These minerals usually occur in a combination of four different modes: (1) replacement of groundmass patches or glass (Fig. **F3**); (2) vesicle linings and/or fillings (Fig. **F4**); (3) partial or complete pseudomorphic replacement of phenocryst phases (Fig. **F5**); and (4) vein or fracture lining and/or infill (Fig. **F6**). Macroscopically, these minerals may exist as coatings on individual pieces. An additional characteristic of alteration in these basalts reported in the *Initial Reports* volume for Leg 187 (Christie, Pederson, Miller, et al., 2001) and developed in greater detail in Thorseth et al., 2003, is microbial alteration recognized by micrometer-width channels penetrating into fresh glass at the contact with palagonite.

T1. Lithologic summary for Leg 187 sites., p. 24

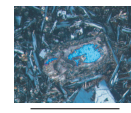
F3. Palagonitization of glass along a fracture, p. 16.



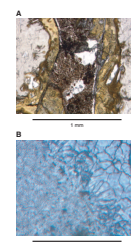
F4. Partially smectite-filled vesicle, p. 17.



F5. Calcite replacing olivine, p. 18.



F6. Silica and calcite veins, p. 19.



Bulk Alteration Characteristics

Cores recovered during Leg 187 were generally grouped into one of three categories (rubble, pillow basalts, or breccia) based on recovery of relatively long oriented pieces, fragment morphology, the presence or absence of oxidation rinds on multiple surfaces, and/or cementing matrix. In the following section we briefly summarize the background alteration features of the core from each site.

Site 1152

Only fragments of slightly altered basalt were recovered from Holes 1152A and 1152B, with no fragments larger than 10 cm (cored 23.7 m, recovered 3.6 m; recovery = 15%). No material indicative of a coherent flow was recovered, and based on multiple surfaces with orange-brown alteration rinds the entire sequence was interpreted to be rubble. Alteration is heterogeneous even within individual fragments, but overall the pieces are only slightly altered. Palagonite is present on all glass surfaces, and fractures and veins are weakly developed (4–14 fractures or veins per meter, average = 7/m recovered core), but low recovery and few large pieces make interpretation based on fracture and vein density tenuous.

Site 1153

Three sections of slightly altered basalt were recovered from Site 1153 (2.7 m recovered from ~8 m basement penetration; recovery = 33%). Virtually all volcanic glass is palagonitized, and fractures and veins are more abundant than in the core from Site 1152 (11–13/m recovered core). Some reconstructed pieces are in excess of 30 cm long and orange-brown oxidation rinds are not as common as seen on fragments from Site 1152; hence, these cores were interpreted to be pillow basalts.

Site 1154

Cores from this site (along with those from Site 1153) are the farthest from the SEIR sampled during Leg 187. In general the alteration intensity is low (as at Site 1153) and the fracture and vein density is also relatively low (1–9/m recovered core; average = 7/m, comparable to Site 1152). Several pieces show no macroscopic evidence of alteration, and even small pieces (that commonly exhibit the most intense effects of alteration) have some fresh surfaces. Recovery was high (for this expedition) at 27%, with a relatively high proportion of large pieces.

Site 1155

Core from Hole 1155A was interpreted to be a lava flow over basaltic rubble, whereas all of the core from Hole 1155B was interpreted as pillow basalt. Structural data for Hole 1155B are likely to be more representative of the site than the values recorded for Hole 1155A, owing to significantly higher recovery and larger pieces in the former. Fracture and vein density in the cores from Hole 1155B is high (7–40/m; average = 19/m). These cores are significantly more altered than any of the earlier cored sites, despite being younger. Hole 1155A had poor recovery (9%), but Hole 1155B recovered nearly 40%.

Site 1156

The upper two cores recovered from Hole 1156A are carbonate-cemented basaltic breccia. Basaltic clasts in the breccia range from pervasively to only slightly altered. Although palagonite is common, fresh basaltic glass is still present in the carbonate matrix and on basalt clasts. Below the breccia and in Hole 1156B, slightly to moderately altered basalt was recovered (recovery = 36%) with some carbonate still present in veins. Fracture and vein density in the basalt (excluding the breccia) ranged 7–24/m (average = ~14/m).

Site 1157

Based on fragment morphology, size, and alteration, all of the material recovered from Hole 1157A is interpreted to be basaltic rubble. Hole 1157B had nearly 30% recovery in rock interpreted to be pillow basalts with a relatively high proportion of oriented pieces. Alteration of core from Hole 1157B is moderate; nearly all pieces of core show evidence of alteration and some is pervasive. Carbonate is common in veins and fracture and vein density in the pillow basalts from Hole 1157B is high (11–32/m; average = 19/m).

Site 1158

Hole 1158A had low recovery of small fragments of basalt with multiple weathered surfaces interpreted to be rubble. Hole 1158B had slightly higher recovery of material interpreted to be pillow basalt. The upper part of the core recovered from Hole 1158C was interpreted to be rubble, but the lower part of the core is coarser grained with a subophitic texture and is interpreted to be a diabase. Alteration is moderate in the rubble from Hole 1158A and the top of Hole 1158C but distinctly less intense in the cores from Hole 1158B and the lower part of Hole 1158C. Fracture and vein density is variable, from 0 to >30 veins and fractures per meter of core.

Site 1159

A single hole at this site returned nearly 30% recovery of overall moderately altered pillow basalt. Fracture and vein density is relatively high (12–30/m; average = 20/m), and alteration is most pronounced in halos along fractures and veins.

Site 1160

Hole 1160A was a shallow hole and only rubble was recovered. Hole 1160B returned relatively high recovery (30%) of basalt with abundant oriented pieces interpreted to represent several flows. Alteration is variable, with most of the core moderately altered; however, several coherent intervals have only slight alteration. Fracture and vein density is also variable (3–30/m) but generally high (average = 18/m).

Site 1161

Two holes at Site 1161 were characterized by poor recovery (<15%) of rubble and breccia with rare pieces of fresh volcanic glass. The basalt fragments recovered are moderately to highly altered. Structural data record a low fracture and vein density (average = 8/m); however, the

low recovery and rare pieces more than a few centimeters long increase the uncertainty in these measurements as representative of the site.

Site 1162

As at Site 1161, all core recovered at Site 1162 is breccia and basaltic rubble with a relatively low fracture and vein density (<4/m) measured in a core with few large pieces. The core is moderately to highly altered. Peculiar to this site is the development of lower greenschist facies alteration in poorly sorted, dolomite-cemented breccia.

Site 1163

At Site 1163 recovery was 33% in pillow basalts with only slight to moderate alteration. Fracture and vein density was relatively high (4–40/m; average = 19/m), and alteration is restricted almost exclusively to the margins of veins and fractures.

Site 1164

The final site occupied during Leg 187 had low recovery (<15%). From Hole 1164A we recovered slightly altered pillow basalt with a low fracture and vein density (6/m). Hole 1164B is all highly to pervasively altered rubble with an average of 10 veins and fractures per meter. Less than 15% of the core recovered from this site consists of pieces large enough to be oriented.

Phenocryst Alteration

Olivine phenocrysts commonly appear to be the most susceptible to alteration, followed by clinopyroxene, and then plagioclase. Olivine and clinopyroxene phenocrysts commonly alter to a combination of Fe oxyhydroxides and smectite. In a few samples, olivine is pseudomorphed by calcite (Fig. F5). Plagioclase phenocryst alteration, though very rare, is manifest as Fe staining along cracks within the crystal (Fig. F7).

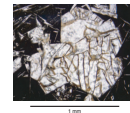
Groundmass Alteration

Alteration in the groundmass is usually restricted to vein, fracture, or chilled margins but can be found in association with altered phenocrysts or filled vesicles. The alteration products are almost exclusively Fe oxyhydroxides and smectite, though in a few samples calcite replaces groundmass (Fig. F3). In samples containing quench glass in the groundmass, the glass is palagonitized.

Vesicle and Vein/Fracture Linings and Fillings

Clays are the most common vesicle lining and infill material (Fig. F4) (though Fe oxyhydroxides and calcite may also be present), whereas veins are dominated by calcite and dolomite. Some veins show multiple generations of infill evidenced by alternating layers of micritic calcite and sparry calcite or calcite and aragonite (Fig. F6). Very fine grained clastic material mixed with micritic carbonate is present as matrix in a few basalt breccia samples.

F7. Plagioclase with Fe-staining along fractures, p. 20.



High-Temperature Alteration

Site 1162 is the only site containing evidence of high-temperature alteration. Greenschist minerals such as talc, chlorite, actinolite (Fig. F8), and albite are found in some basalt clasts, indicating temperatures of metamorphism between 150° and 250°C (Alt et al., 1996). These clasts are interpreted to have eroded out of a nearby fault ridge and transported to the area where they later became part of the breccias (Shipboard Scientific Party, 2001).

Elemental Changes Associated with Alteration

The major element analyses of altered basalts from Leg 187 are presented in Table T2. The table includes data reported from SRM and duplicates as unknowns. Volume change during a reaction can cause an apparent dilution or concentration of a component in the altered rock compared to its fresh equivalent. Gresens (1967) presents a method for determining volume change based on the concept that if immobile elements can be identified they can be used to determine if any volume change has taken place. From this estimate of volume change, gains or losses of chemical components can be calculated based on the volume change. This method was modified by Grant (1986) to relate the concentration of a component in an altered rock to that in its unaltered precursor through a mass change term such that

$$C_i^A = (M^o/M^A) (C_i^o + C_i),$$

where

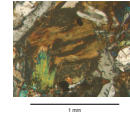
- C_i^A = concentration of component i in the altered sample,
- M^o = mass of the fresh sample,
- M^A = mass of the altered sample,
- C_i^o = the concentration of component i in the fresh sample, and
- C_i = change in concentration of component i from the fresh to altered sample.

Plotting C_i^A against C_i^o for each component yields an isocon diagram. Some component concentrations must be scaled up or down to fit on a single plot of concentrations of elements in altered rock vs. their concentration in a fresh precursor. Immobile components ($C_i = 0$) define the isocon (same concentration) or line going through the origin connecting immobile component points. The slope of the isocon defines the mass change term (M^o/M^A). A value of 1 implies no change, whereas values greater or less than 1 indicate mass addition and depletion, respectively. Once the mass change term is known, the actual or true gains and losses of the other species can be calculated using the equation above.

Baumgartner and Olsen (1995) demonstrate a drawback of Grant's method by showing that arbitrary scaling of component concentrations influences the slope of the isocon, which can introduce error in the calculations and lead to misinterpretation in gains and losses. Instead, they suggest using a statistical approach involving averages and standard deviations in component values of a sample set to construct the isocon.

Humphris et al. (1998) present a simpler method wherein the concentration of each component in the fresh sample and counterpart altered sample is scaled such that the sum of the squares of the scaled

F8. Actinolite replacing clinopyroxene, p. 21.



T2. Bulk rock chemistry of altered samples, p. 25.

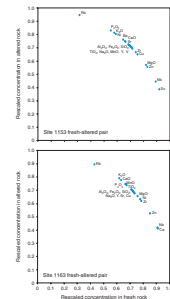
concentrations, for each component, equals 1. The data points are plotted such that the x- and y-values are the scaled values of a component in the fresh sample and altered sample, respectively. Scaling each component uses the general equation of a circle. By dividing the x- and y-values by the square root of the sum of the squares of these values, the data plot along an arc with a radius of 1.

This method eliminates errors introduced by visual effects. Components that cluster together along the arc are interpreted as having geochemically similar behavior. In general, they are considered to be relatively immobile (Humphris et al., 1998). By considering each of these elements' behavior in other experiments or studies and applying knowledge about how each element is likely to behave, a suitable immobile element is chosen to calculate the mass change term. Elements that plot above the cluster along the arc are interpreted as having a concentration increase during the reaction. Conversely, elements that plot below the cluster along the arc are those that are interpreted to have a decrease in concentration during the reaction. An additional complication to using this method is that we cannot state with certainty that our sample pairs originated from the same lava flow. Fresh and altered samples were paired according to their proximity in the core and lithology (i.e., plagioclase-olivine-phyric basalt).

We determined from this analysis that aluminum was an immobile component at 12 of 13 sites (Site 1162 was not included because no fresh whole-rock samples from this site were analyzed). Example isocon plots are shown in Figure F9. Using aluminum as an immobile component, we calculate the mass change term for 31 fresh-altered pairs representative of the lithologic units at each of the sites (Table T3). All but three of the M^o/M^A values range from 0.92 to 1.08; thus, very little mass change appears to have taken place. The three samples with M^o/M^A significantly greater than 1 were all from samples of breccia or drilling rubble and are not considered representative of mass change due to low-temperature alteration.

According to Alt (1995), we should expect alkalis like K, Na, and Rb to be elevated in altered basalts. In these samples, Rb is commonly elevated and K is enriched in the basalts from about half of the holes drilled, but Na is rarely so. This suggests alteration took place at $<150^\circ\text{C}$ as experimental data indicate K can be extracted from seawater by basalts during oxidative alteration at temperatures $<70^\circ\text{C}$ but that K is lost from basalts during alteration at temperatures $>150^\circ\text{C}$ (Seyfried and Bischoff, 1979; Seyfried, 1987). Bulk Mg loss is not evident, again indicative that reactions $>150^\circ\text{C}$, which enrich magnesium in altered basalts (Alt, 1995), were not common during alteration of these basalts. Ni is most commonly lost during alteration (at Sites 1152, 1156, 1157, 1159, 1160, 1161, 1163, and 1164) or relatively immobile (Sites 1154, 1155, and 1158). The phenocryst phase that most commonly shows evidence of alteration is olivine; even in slightly altered rocks the olivine can be pervasively altered. At all of the sites where Ni was lost, olivine in thin section shows evidence of alteration. At the three sites where olivine was relatively immobile, the basalts were either aphyric or only incipiently altered (with olivine only altered when it was adjacent to fractures) or both. In one instance (Site 1153; see Fig. F9), Ni appeared to be slightly elevated in the altered rocks. For most of our altered samples, we selected an analysis from the shipboard data set for a fresh bulk rock from as close as possible to the location of our sample for comparison. In this case, the closest fresh sample was from a different section of

F9. Isocon plots, p. 22.



T3. Estimated mass change, lithology, and alteration intensity, p. 26.

core, and as part of a wash core may not be representative of the primary composition of the altered basalt we analyzed.

Correlation between Chemical Components, Secondary Mineralogy, and Age

Whereas we recognize that statistical correlations are empirical and cannot be used to infer causality, we can use them to test the strength of a relationship in the case where a relationship is known or expected to exist. Furthermore, the absence of a statistical correlation does not necessarily imply that two variables are not related. The absence may indicate that some other variable is masking the relationship between them. In any case, correlation coefficients, even within a 95% confidence limit, must still be interpreted with caution.

Correlation coefficients are given for Leg 187 altered basalts ($n = 45$) in Table T4. The correlation coefficients for the oxides P_2O_5 , TiO_2 , MnO , and Cr_2O_3 are not considered as reliable as the other major element oxides, owing to the greater amount of uncertainty in their reported values. From these correlation coefficients, we surmise that as loss on ignition (LOI) increases (our best estimate of water content and an indicator of alteration of primary phases and glass to hydrated phases) MgO , Fe_2O_3 , SiO_2 , and MnO decrease and CaO and K_2O increase. Similarly, as intensity of alteration increases (as estimated by the abundance of secondary phases) MgO and SiO_2 decrease. MgO loss is commonly attributed to alteration of olivine to minerals formed at low temperatures (usually clays) and uptake of Mg by seawater. H_2O is added to the rock as a component in the clay and hydrated basaltic glass in the groundmass (palagonite). In this study, MgO (weight percent) and SiO_2 (weight percent) loss, LOI (weight percent) gain, and the abundance of secondary minerals (modal percent) are used as indicators of the intensity of alteration.

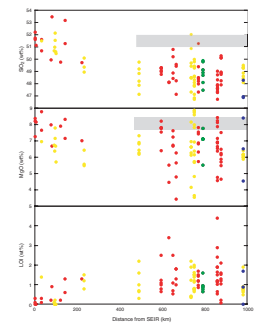
The premise of this investigation was the shipboard observation that there did not appear to be an obvious relationship between the intensity of alteration and the age of the rocks. Our statistical analysis supports this observation, in that there is no significant correlation between age and any of our indicators of alteration intensity.

Inasmuch as we could interpret no statistical correlation between the age of the basalts sampled and the intensity of alteration, we turn to visual representations of the data to see if any trends are apparent. Figure F10 shows three indicators of alteration intensity plotted with respect to distance from the spreading axis. Decreases in silica and magnesium as well as an increase in LOI are evident in samples from the dredge collection, which range from 0 to 7 Ma. More subtle, but still recognizable, is an indication of increasing alteration of cored basalts with increasing distance from the spreading axis. Although there is considerable scatter in all these plots owing to heterogeneity in alteration intensity even within sites, we can still make the following observations.

As expected, or at least hoped, there is a direct relationship between LOI and the abundance of secondary minerals, providing support for the quality of our petrographic analyses. For all sites, samples with <1 wt% LOI have <10% alteration phases. Similarly, all samples with >30% alteration have >2.5 wt% LOI. At most sites where rubble was recovered from one hole and pillow lavas from a second hole, the lavas interpreted to be from flows contain higher SiO_2 (less of an alteration signature). The exception is Site 1155, where all samples were at least moder-

T4. Correlation coefficients for data for altered samples, p. 27.

F10. Geochemical data relative to distance from SEIR, p. 23.



ately altered. This relationship does not hold as well for MgO. Probably the most interesting observation we make is that the trends of decreasing SiO₂ and MgO and increasing LOI do not seem to hold for the three oldest sites, consistent with the shipboard observation and our statistical analysis that show no systematic relationship between degree of alteration and age of the crust.

In order to resolve these contrasting observations and interpretations, we appeal to structural information determined from shipboard core descriptions for a possible explanation. As reported above, one of the parameters measured on all of the cores recovered during Leg 187 was the number of fractures and veins per meter of core as an indicator of fracture and vein density. Fractures are the primary conduits for water penetration into the basalts erupted along a spreading axis and thus are probably the most critical parameter in accelerating or enhancing the possibility of alteration.

If we disregard the low fracture and vein density values for sites where recovery was low or there was not significant recovery of oriented pieces of core, all sites between 14 and 24.5 Ma have fracture and vein density values of ~20/m. Cores from the three oldest sites have 12 or fewer fractures and veins per meter. Whereas it might be presumptuous to put much stock in volumetric data with recovery as low as we experienced during Leg 187, we have yet to develop an alternative hypothesis. This study suggests that indeed alteration intensity does increase as rocks age and move off axis, and whereas this is particularly pronounced in rocks younger than 14 Ma, there still appears to be evidence of continued increasing alteration through rocks of at least 24 Ma. The lower indices of alteration present in the oldest rocks we sampled, however, suggest two alternatives. Either permeability (as evidenced by fracture and vein density) plays a more significant role in the alteration history of the oceanic crust at the AAD than age or the subtle indication of increasing alteration we interpret in rocks from 14 to 24 Ma is coincidental (as suggested by the range in alteration indices present in dredge samples) and the intensity of alteration is fixed early in the evolution of the crust.

ACKNOWLEDGMENTS

The authors wish to thank Harald Furnes, Martin Fisk, David Christie, and Rolf Pedersen for reviews that improved this manuscript. This research used samples and/or data provided by the Ocean Drilling Program (ODP). ODP is sponsored by the U.S. National Science Foundation (NSF) and participating countries under management of Joint Oceanographic Institutions (JOI), Inc. Funding for this research was provided by United States Science Support Program.

REFERENCES

- Alt, J.C., 1995. Subseafloor processes in mid-ocean ridge hydrothermal systems. In Humphris, S.E., Zierenberg, R., Mullineaux, L., and Thomson, R. (Eds.), *Seafloor Hydrothermal Systems: Physical, Chemical, Biological and Geological Interactions within Hydrothermal Systems*. Geophys. Monogr., 91:85–114.
- Alt, J.C., Honnorez, J., Laverne, C., and Emmermann, R., 1986. Hydrothermal alteration of a 1 km section through the upper oceanic crust, Deep Sea Drilling Project Hole 504B: mineralogy, chemistry, and evolution of seawater-basalt interactions. *J. Geophys. Res.*, 91:10309–10335.
- Alt, J.C., Laverne, C., Vanko, D.A., Tartarotti, P., Teagle, D.A.H., Bach, W., Zuleger, E., Erzinger, J., Honnorez, J., Pezard, P.A., Becker, K., Salisbury, M.H., and Wilkens, R.H., 1996. Hydrothermal alteration of a section of upper oceanic crust in the eastern equatorial Pacific: a synthesis of results from Site 504 (DSDP Legs 69, 70, and 83, and ODP Legs 111, 137, 140, and 148.) In Alt, J.C., Kinoshita, H., Stokking, L.B., and Michael, P.J. (Eds.), *Proc. ODP, Sci. Results*, 148: College Station, TX (Ocean Drilling Program), 417–434.
- Anderson, R.N., Langseth, M.G., and Sclater, J.G., 1977. The mechanisms of heat transfer through the floor of the Indian Ocean. *J. Geophys. Res.*, 82:3391–3409.
- Baumgartner, L.P., and Olsen, S.N., 1995. A least-squares approach to mass transport calculations using the isocon method. *Econ. Geol.*, 90:1261–1270.
- Cande, S.C., LaBrecque, J.L., Larson, R.L., Pitmann, W.C., III, Golovchenko, X., and Haxby, W.F., 1989. *Magnetic Lineations of the World's Ocean Basins*. AAPG Map Ser., 13.
- Christie, D.M., Pedersen, R.B., Miller, D.J., et al., 2001. *Proc. ODP, Init. Repts.*, 187 [CD-ROM]. Available from: Ocean Drilling Program, Texas A&M University, College Station TX 77845-9547, USA.
- Christie, D.M., West, B.P., Pyle, D.G., and Hanan, B.B., 1998. Chaotic topography, mantle flow and mantle migration in the Australian–Antarctic Discordance. *Nature*, 394:637–644.
- Davis, E.E., Fisher, A.T., Firth, J.V., et al., 1997. *Proc. ODP, Init. Repts.*, 168: College Station, TX (Ocean Drilling Program).
- Davis, E.E., Mottl, M.J., Fisher, A.T., et al., 1992. *Proc. ODP, Init. Repts.*, 139: College Station, TX (Ocean Drilling Program).
- Delaney, J.R., Robigou, V., McDuff, R.E., and Tivey, M.K., 1992. Geology of a vigorous hydrothermal system on the Endeavour Segment, Juan de Fuca Ridge. *J. Geophys. Res.*, 97:19663–19682.
- Embley, R.W., and Chadwick, W.W., 1994. Volcanic and hydrothermal processes associated with a recent phase of sea floor spreading at the northern cleft segment: Juan de Fuca Ridge. *J. Geophys. Res.*, 99:4741–4760.
- Forsyth, D.W., Ehrenbard, R.L., and Chapin, S., 1987. Anomalous upper mantle beneath the Australian–Antarctic Discordance. *Earth Planet. Sci. Lett.*, 84:471–478.
- Fouquet, Y., Zierenberg, R.A., Miller, D.J., et al., 1998. *Proc. ODP, Init. Repts.*, 169: College Station, TX (Ocean Drilling Program).
- Grant, J.A., 1986. The isocon diagram—a simple solution to Gresen's equation for metasomatic alteration. *Econ. Geol.*, 81:1976–1982.
- Gresens, R.L., 1967. Composition-volume relationships of metasomatism. *Chem. Geol.*, 2:47–65.
- Hammond, S.R., 1990. Relationships between lava types, seafloor morphology, and the occurrence of hydrothermal venting in the ASHES vent field of Axial Volcano. *J. Geophys. Res.*, 95:12875–12893.
- Humphris, S.E., Alt, J.C., Teagle, D.A.H., and Honnorez, J.J., 1998. Geochemical changes during hydrothermal alteration of basement in the stockwork beneath the active TAG hydrothermal mound. In Herzig, P.M., Humphris, S.E., Miller, D.J., and

- Zierenberg, R.A. (Eds.), *Proc. ODP, Sci. Results*, 158: College Station, TX (Ocean Drilling Program), 255–276.
- Humphris, S.E., Herzig, P.M., Miller, D.J., et al., 1996. *Proc. ODP, Init. Repts.*, 158: College Station, TX (Ocean Drilling Program).
- Marks, K.M., Vogt, P.R., and Hall, S.A., 1990. Residual depth anomalies and the origin of the Australian–Antarctic Discordance Zone. *J. Geophys. Res.*, 95:17325–17337.
- Palmer, J., Sempéré, J.-C., Christie, D.M., and Phipps-Morgan, J., 1993. Morphology and tectonics of the Australian–Antarctic Discordance between 123°E and 128°E. *Mar. Geophys. Res.*, 15:121–152.
- Pyle, D.G., Christie, D.M., Mahoney, J.J., and Duncan, R.A., 1995. Geochemistry and geochronology of ancient southeast Indian and southwest Pacific seafloor. *J. Geophys. Res.*, 100:22261–22282.
- Sclater, J.G., Jaupart, C., and Galson, D., 1980. The heat flow through oceanic and continental crust and the heat loss of the Earth. *Rev. Geophys. Space Phys.*, 18:269–311.
- Sempéré, J.-C., Palmer, J., Christie, D.M., Phipps-Morgan, J., and Shor, A.N., 1991. Australian–Antarctic discordance. *Geology*, 19:429–432.
- Seyfried, W.E., 1987. Experimental and theoretical constraints on hydrothermal alteration processes at mid-ocean ridges. *Annu. Rev. Earth Planet. Sci.*, 15:317–335.
- Seyfried, W.E., and Bischoff, J.L., 1979. Low temperature basalt alteration by seawater: an experimental study at 70°C and 150°C. *Geochim. Cosmochim. Acta.*, 43:1937–1947
- Shipboard Scientific Party, 2001. Site 1162. In Christie, D.M., Pedersen, R.B., Miller, D.J., et al., *Proc. ODP, Init. Repts.*, 187, 1–46 [CD-ROM]. Available from: Ocean Drilling Program, Texas A&M University, College Station TX 77845-9547, USA.
- Thorseth, I.H., Pedersen, R.B., and Christie, D.M., 2003. Microbial alteration of 0–30-ma seafloor and sub-seafloor basaltic glasses from the Australian–Antarctic Discordance. *Earth Planet. Sci. Lett.*, 215:237–247.
- Vogt, P.R., Cherkis, N.Z., and Morgan, G.A., 1983. Project investigator—1. Evolution of the Australia–Antarctic Discordance deduced from a detailed aeromagnetic study. In Oliver, R.L., James, P.R., and Jago, J.B. (Eds.), *Antarctic Earth Science*. Antarctic Earth Sci., [Pap.—Int. Symp.], 4th, 608–613.
- Weissel, J.K., and Hayes, D.E., 1971. Asymmetric seafloor spreading south of Australia. *Nature*, 231:518–522.
- West, B.P., 1997. Mantle flow and crustal accretion in and near the Australian–Antarctic Discordance [Ph.D. thesis]. Univ. of Washington, Seattle.
- West, B.P., Sempéré, J.-C., Pyle, D.G., Phipps-Morgan, J., and Christie, D.M., 1994. Evidence for variable upper mantle temperature and crustal thickness in and near the Australian–Antarctic Discordance. *Earth Planet. Sci. Lett.*, 128:135–153.

Figure F1. Regional map of the Southeast Indian Ocean (after Pyle et al., 1995) showing magnetic lineations (Cande et al., 1989), the Australian-Antarctic Discordance (AAD), and DSDP (large solid circles with number) and ODP (small solid circles) sites. The broad gray “V” is the approximate trace of the regional depth anomaly. Inset box is the area of operations for Leg 187, and the location of Figure F2, p. 15.

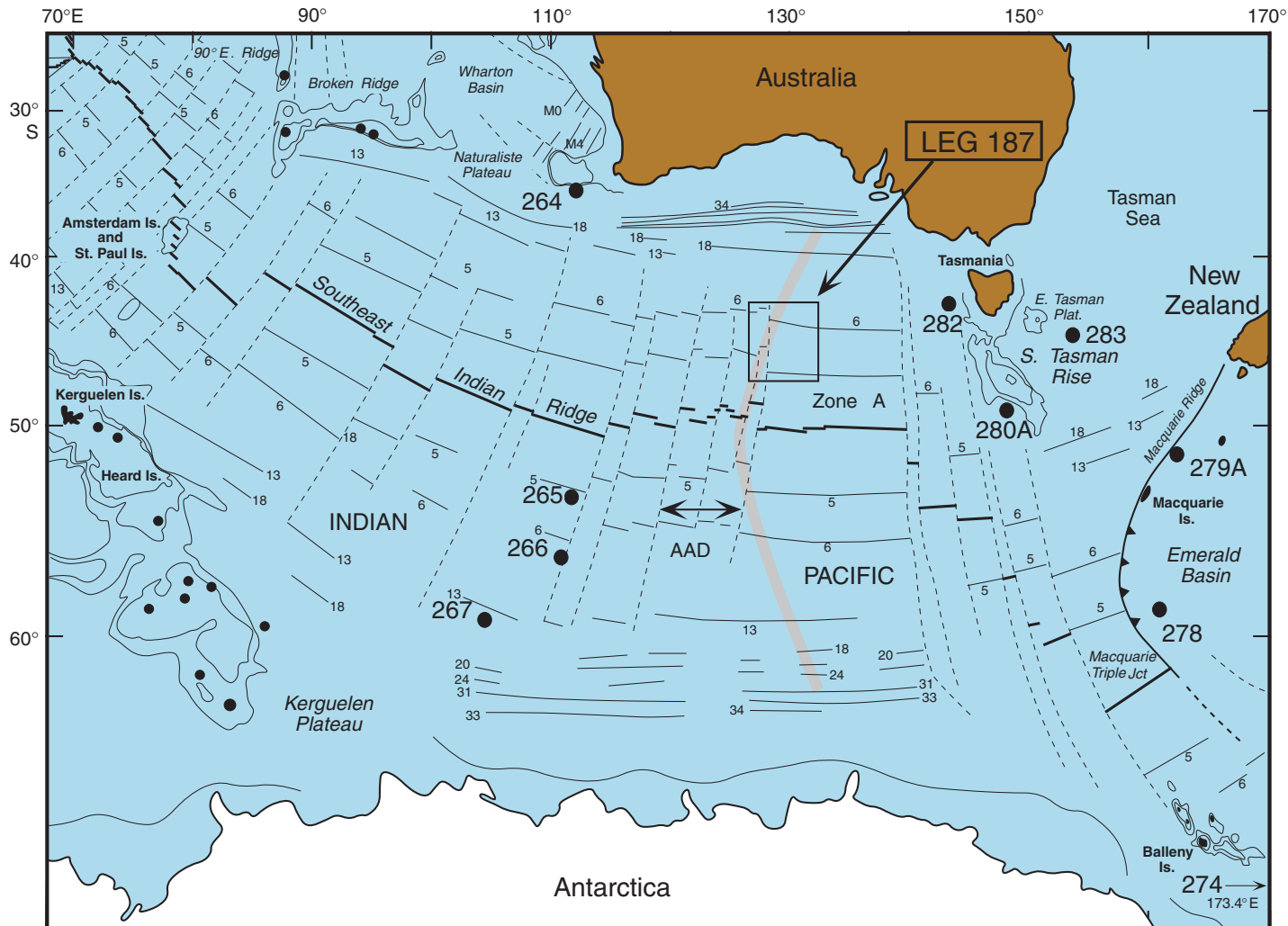


Figure F2. Site locations for Leg 187 in relation to seafloor isochrons (after Vogt et al., 1983) in 1-Ma intervals. The Southeast Indian Ridge (SEIR) crest is represented by the heavy black line running east-west, transform faults in the AAD are indicated by light, roughly north-south oriented offsets in isochrons. Small circles represent dredge locations. Red symbols = sites classified as Indian mantle MORB source, yellow = Pacific mantle, blue = transitional, and green = mixed.

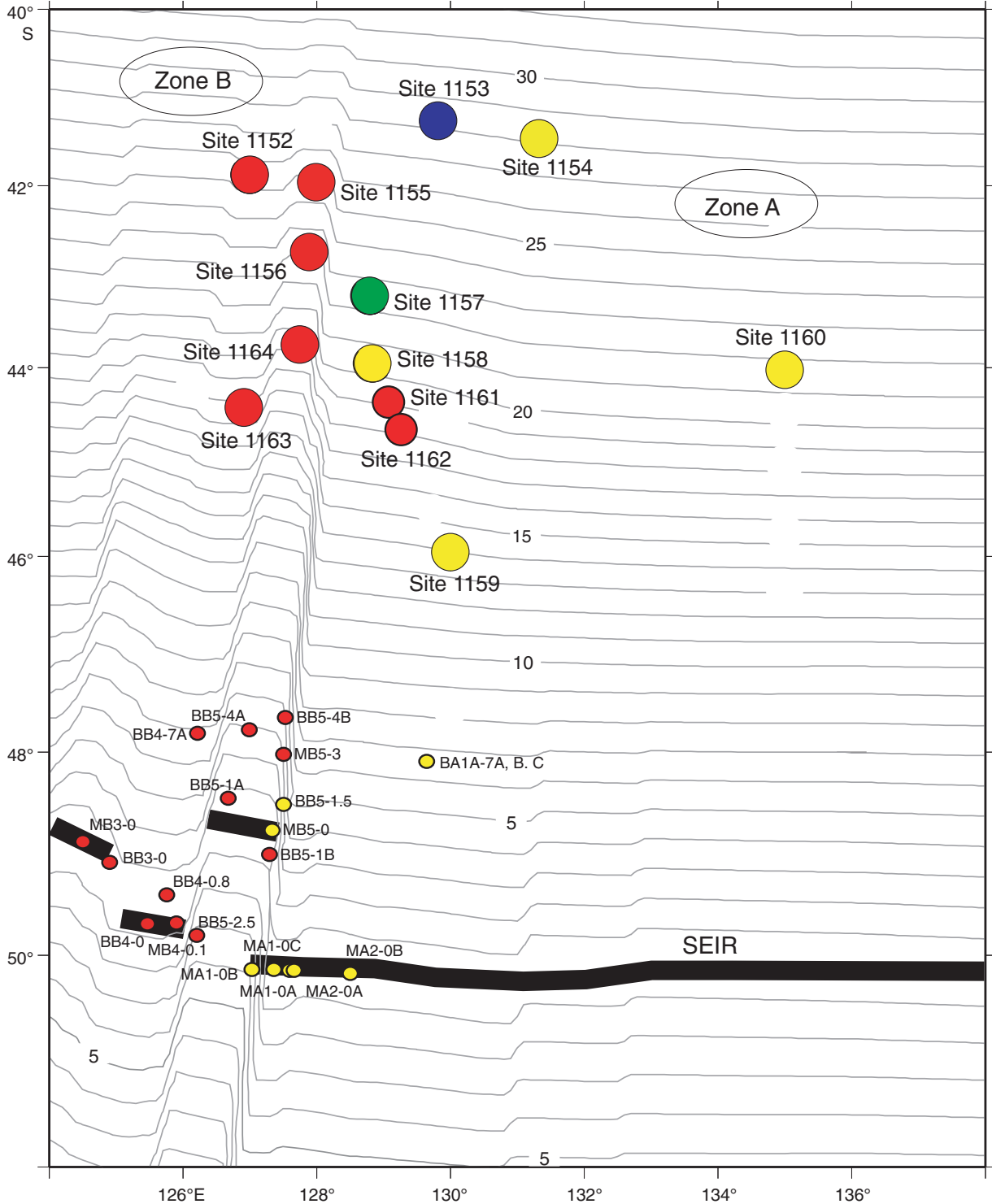
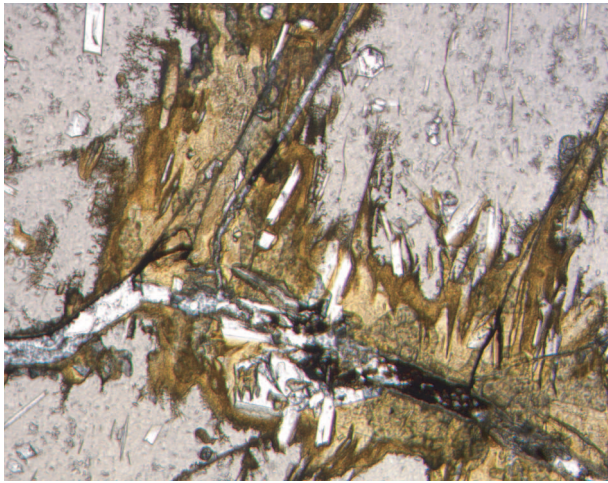


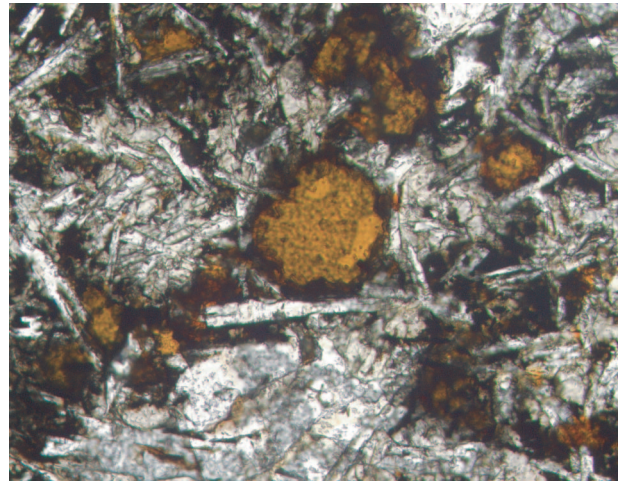
Figure F3. A. Palagonitization of glass along a fracture (Sample 187-1155B-6R-3, 135–138 cm); transmitted light. B. Smectite replacing groundmass glass (Sample 187-1154A-5R-1, 58–62 cm); transmitted light. C. Calcite replacing groundmass glass (Sample 187-1164A-4R-1, 22–24 cm); cross-polarized light.

A



1 mm

B



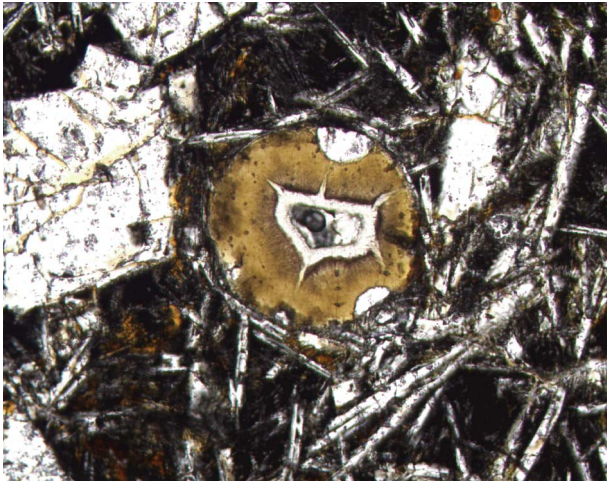
1 mm

C



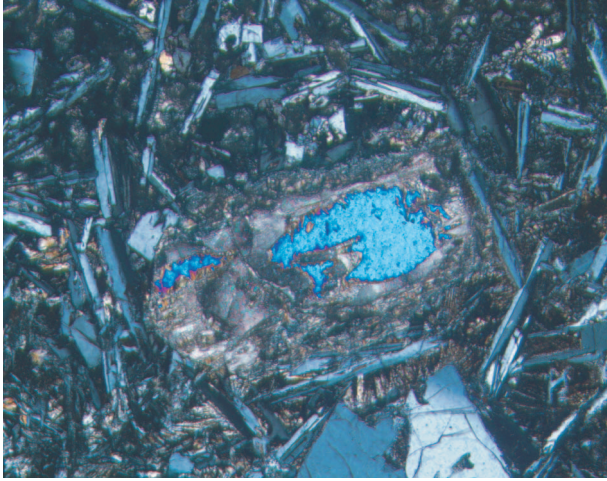
0.5 mm

Figure F4. Vesicle partially filled with golden-brown smectite (Sample 187-1156A2R-1, 8–12 cm); transmitted light.



1 mm

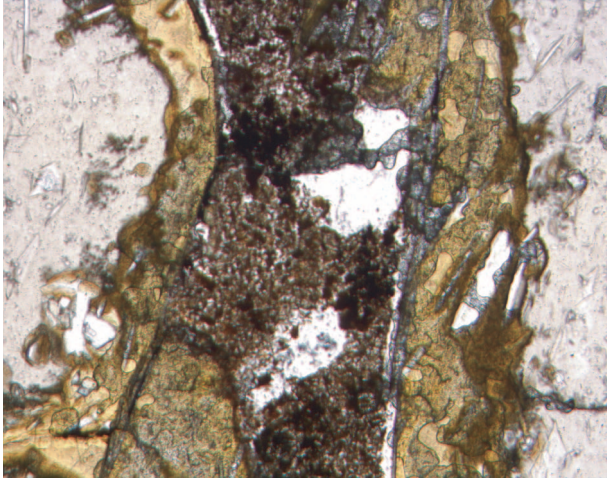
Figure F5. Calcite replacement of olivine (Sample 187-1157B-8R-2, 5–59 cm); cross-polarized light.



1 mm

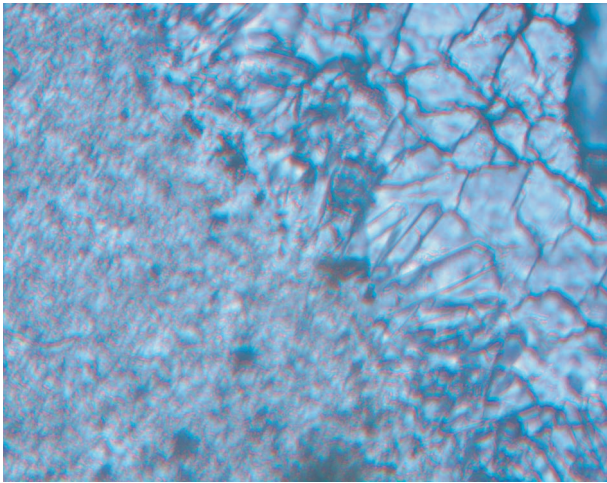
Figure F6. (A) Silica vein with a palagonitized halo cutting through volcanic glass (Sample 187-1155B-6R-3, 135–138 cm) and (B) aragonite crystals along a calcite vein wall (Sample 187-1155B-2R-1, 68–71 cm); both transmitted light.

A



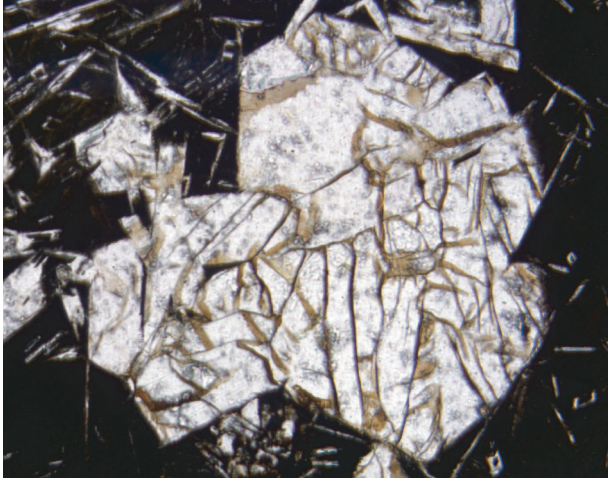
1 mm

B



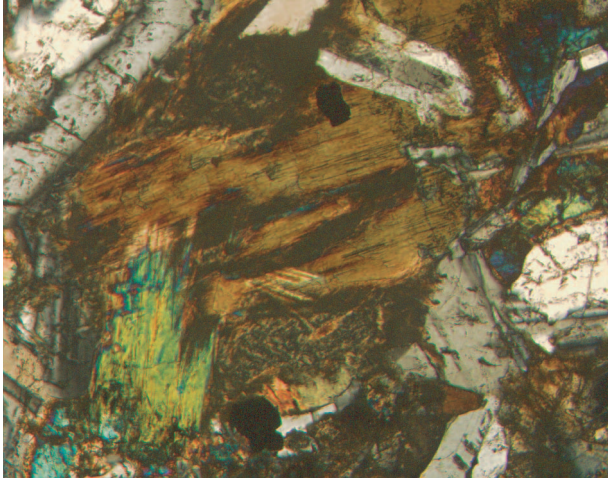
0.2 mm

Figure F7. Plagioclase with Fe-staining along fractures (Sample 187-1156A-3R-1, 5–9 cm); transmitted light.



1 mm

Figure F8. Actinolite replacing clinopyroxene (Sample 187-1162A-5R-1, 25–28 cm); cross-polarized light.



1 mm

Figure F9. Examples of isocon plots for two sites from Leg 187.

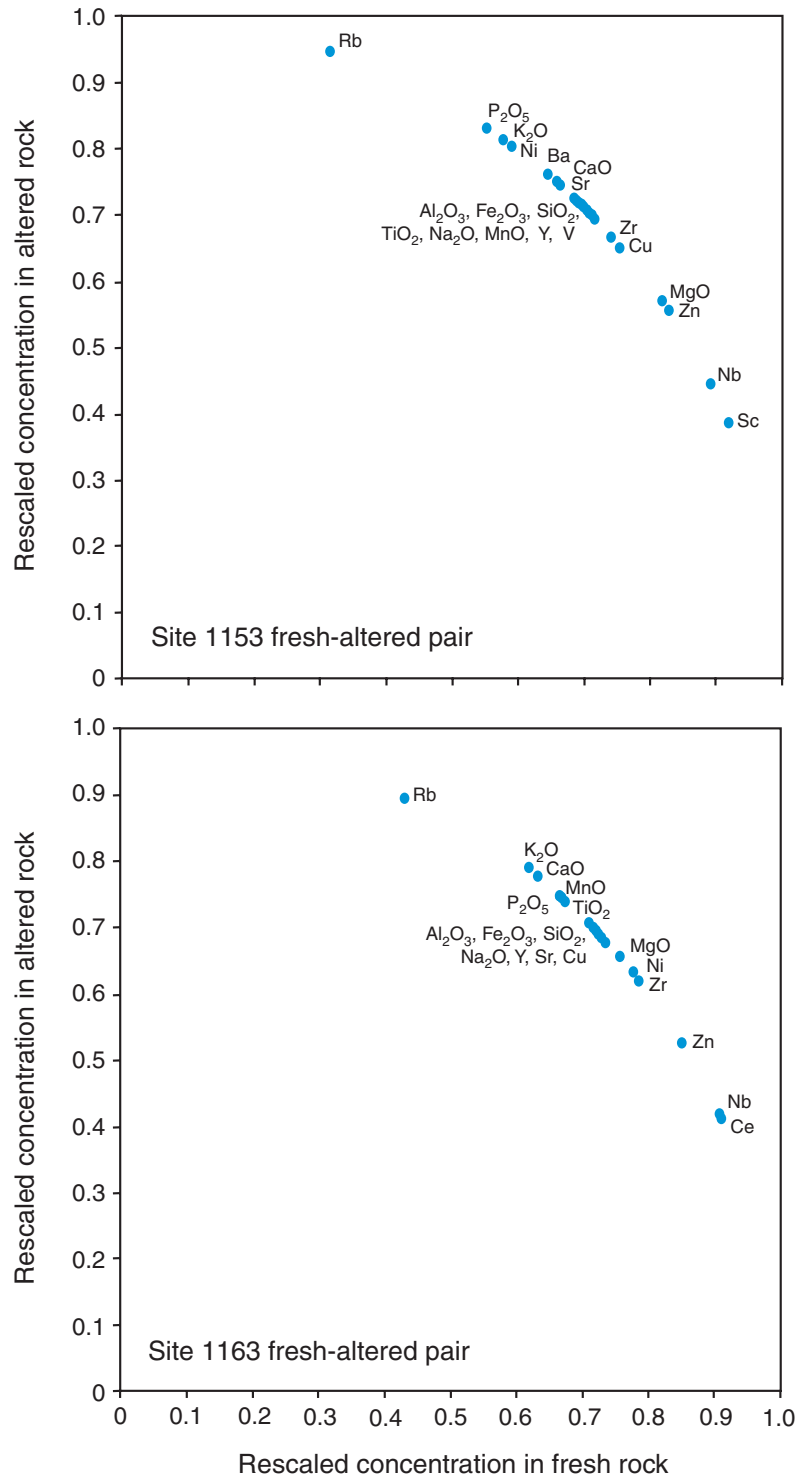


Figure F10. Geochemical data plotted relative to distance from the Southwest Indian Ridge (SEIR). Red = sites classified as having an Indian mantle MORB source, yellow = Pacific mantle MORB source sites, blue = transitional mantle MORB source sites, green = sites with mixed sources. Gray shaded areas = average fresh basalt compositions from Leg 187.

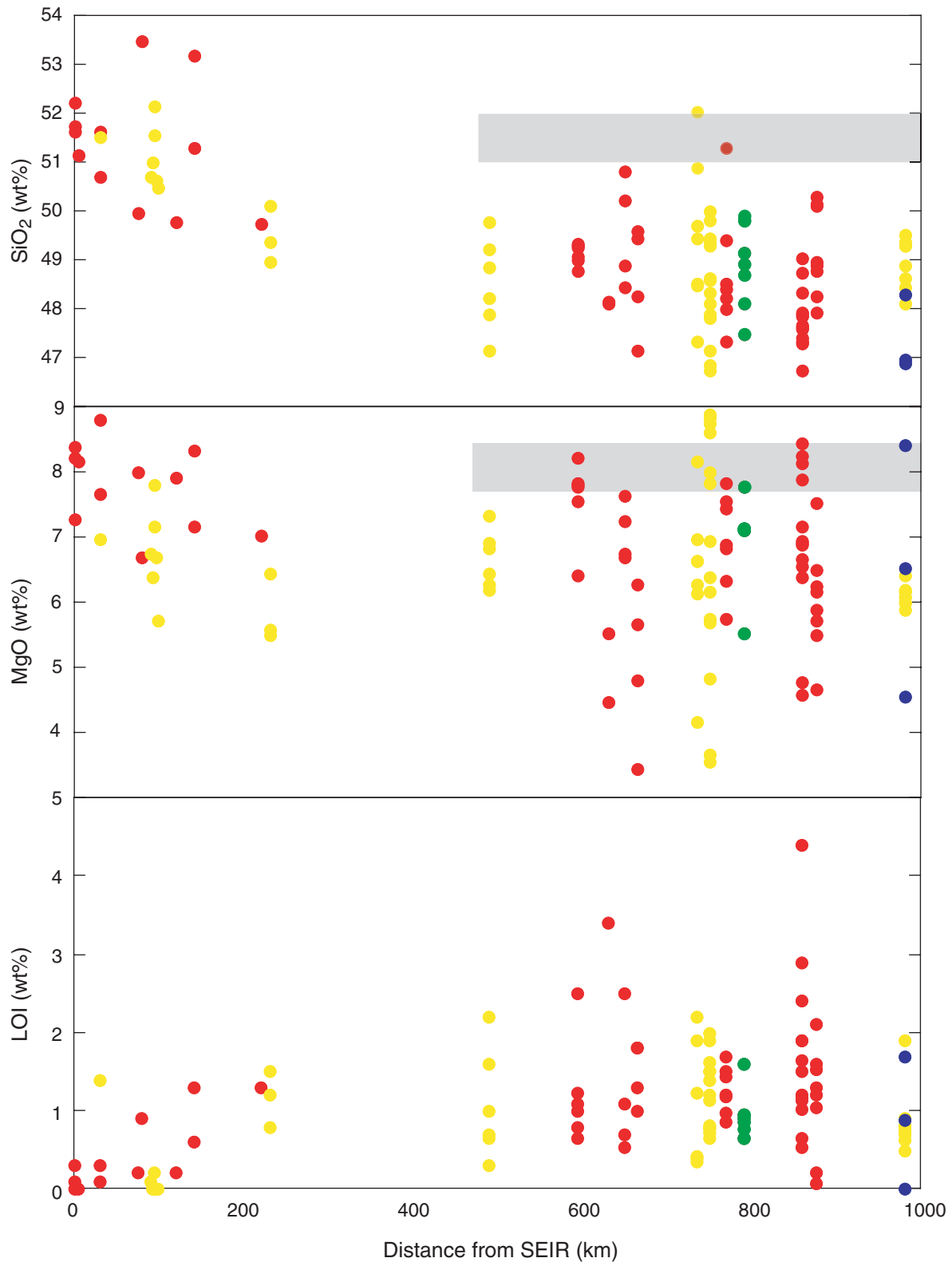


Table T1. Lithologic summary for Leg 187 sites.

Hole	Age (Ma)	Recovery (%)	Average fracture and vein density (N/m)	Lithology	Average alteration intensity
1153A	28	24	12.2	Aphyric basalt	Slight
1154A	28	27	6.8	Moderately plagioclase-olivine phyric basalt	Slight
1152A	25	5.3	6.7	Aphyric basalt	Slight
1152B	25	15.1	7.8	Aphyric to moderately plagioclase phyric basalt	Slight
1155A	24.5	8.9	7.1	Aphyric to moderately plagioclase-olivine phyric basalt and basaltic rubble	Moderate
1155B	24.5	39.5	19.6	Moderately plagioclase-olivine phyric basalt	Moderate
1157A	22.5	17.8	14	Basaltic breccia	Moderate
1157B	22.5	29	20	Moderately plagioclase-olivine phyric basalt	Moderate
1156A	22	55.3	15	Sparsely plagioclase-olivine phyric basalt and moderately plagioclase-olivine phyric basaltic breccia	Moderate
1156B	22	29.5	14	Moderately to highly plagioclase-olivine phyric basalt	Moderate
1160A	21.5	8.4	21	Aphyric basaltic rubble	Moderate to high
1160B	21.5	28.8	17.3	Aphyric to moderately plagioclase-olivine phyric basalt	Moderate to high
1158A	21	5.9	8.6	Aphyric to sparsely olivine-plagioclase phyric basalt	Slight to moderate
1158B	21	10.7	16.6	Aphyric to sparsely olivine-plagioclase phyric basalt	Slight to moderate
1158C	21	17.1	7.2	Aphyric to sparsely olivine-plagioclase phyric basalt and diabase	Slight to moderate
1161A	19	10	8.1	Sparsely to moderately plagioclase-olivine phyric basaltic rubble	Moderate to high
1161B	19	15	7.7	Sparsely to moderately plagioclase-olivine phyric basaltic rubble	Moderate to high
1164A	18.5	11.4	6.1	Aphyric basalt	Slight to pervasive
1164B	18.5	16.2	9.7	Basaltic rubble	Slight to pervasive
1162A	18	8.2	9.9	Basaltic rubble	High to pervasive
1162B	18	16.9	1.3	Basaltic breccia	High to pervasive
1163A	17	33.3	18.6	Aphyric to moderately plagioclase-olivine phyric basalt	Slight to moderate
1159A	14	28.7	20	Aphyric basalt	Slight to moderate

Note: *N* = number.

Table T2. Bulk rock chemistry of altered samples from Leg 187 and the Oregon State University Australian Antarctic Discordance dredge collection. (This table is available in an [oversized format](#).)

Table T3. Estimated mass change terms, lithology, and alteration intensity of samples from Leg 187.

Core, section, interval (cm)	Mass change term	Lithology	Alteration characteristics	Secondary mineralogy (modal%)
187-				
1152A-1R-1, 73-77				
1152A-1R-1, 21-25	1.02	Aphyric basalt	Alteration halos	25
1152A-1R-1, 73-77	1.05	Aphyric basalt	1.5-cm-thick brown alteration rind	20
1152B-4R-1, 21-24	0.98	Aphyric basalt	Only slightly altered	38
1152B-6R-1, 20-25	1	Sparsely plagioclase clinopyroxene phyric basalt	Thin oxidation rind	10
1153A-8R-2, 10-13	1.04	Aphyric basalt	2- to 3-cm-thick oxidation rind	14
1154A-2R-1, 40-42	0.99	Moderately plagioclase olivine phyric basalt	1-cm-thick oxidation halo	13
1154A-4R-2, 10-12	1.03	Moderately plagioclase olivine phyric basalt	1-cm-thick oxidation halo	15
1154A-7R-1, 65-68	1.02	Sparsely plagioclase olivine phyric basalt	2-cm-thick alteration halo	25
1154A-8R-1, 101-104	1.03	Moderately plagioclase olivine phyric basalt	Weathered surface	15
1154A-9R-1, 33-36	0.99	Moderately plagioclase olivine phyric basalt	2-cm-thick alteration halo	10
1155A-3R-1, 15-18	1	Sparsely plagioclase olivine phyric basalt	Barely altered	10
1155B-5R-1, 112-116	1.07	Moderately plagioclase olivine phyric basalt	Patchy but abundant groundmass alteration	45
1155B-5R-2, 4-9	1.08	Moderately plagioclase olivine phyric basalt	8-cm-thick alteration halo	55
1155B-6R-1, 82-87	1.04	Moderately plagioclase olivine phyric basalt	Patchy but abundant groundmass alteration	53
1155B-7R-1, 91-95	1.02	Moderately plagioclase olivine phyric basalt	Fractures have alteration halos, patchy groundmass alteration	63
1155B-8R-1, 98-103	1.08	Moderately plagioclase olivine phyric basalt	Moderate overall alteration	45
1165A-3R-1, 96-101	0.93	Moderately plagioclase olivine phyric basalt	Highly fractured piece, broad alteration halos	35
1165B-2R-1, 10-16	0.97	Moderately plagioclase olivine phyric basalt	Only slightly altered	17
1165B-3R-1, 29-32	0.99	Moderately plagioclase olivine phyric basalt	Only slightly altered	8
1165B-6R-1, 80-82	1.06	Moderately plagioclase olivine phyric basalt	Patchy groundmass alteration	12
1157A-2R-1, 33-35	1.33	Basalt-carbonate breccia	Moderate overall alteration	35
1157A-3R-1, 66-70	1.05	Basalt-carbonate breccia	Moderate overall alteration	43
1157A-4R-1, 7-12	1.05	Sparsely plagioclase olivine phyric basalt	Only slightly altered	20
1157B-2R-1, 100-104	0.93	Moderately plagioclase olivine phyric basalt	Alteration halos	40
1157B-3R-2, 93-97	1.01	Sparsely plagioclase olivine phyric basalt	Only slightly altered	20
1158A-2R-1, 38-41	0.98	Sparsely plagioclase olivine phyric basalt	Moderately altered, abundant clay	42
1158B-4R-1, 2-5	1.05	Sparsely plagioclase olivine phyric basalt	Moderate to highly altered, oxidized margins	50
1158C-2R-2, 15-19	0.98	Diabase	Olivine completely altered, plagioclase Fe-stained	55
1159A-1W-CC, 14-18	1.02	Aphyric basalt	Orange-brown oxidation halo	20
1159A-3R-1, 19-24	0.98	Aphyric basalt	Moderately altered, abundant fractures	40
1159A-5R-1, 10-15	1.02	Aphyric basalt	Patchy groundmass alteration	30
1159A-7R-2, 6-10	0.92	Aphyric basalt	1-cm-thick oxidation halo	15
1160B-7R-1, 71-75	0.99	Moderately plagioclase phyric basalt	Alteration halos along fractures	30
1160B-7R-2, 18-23	1	Moderately plagioclase phyric basalt	Slightly altered	5
1161A-3R-1, 16-21	1.14	Basaltic rubble	Olivine completely altered, plagioclase Fe-stained	48
1161A-3R-1, 116-120	1	Basaltic rubble	Pervasive alteration	20
1161A-4R-1, 98-103	0.98	Basaltic rubble	Pervasive groundmass alteration	65
1161B-3R-1, 8-11	0.99	Basaltic rubble	Slightly altered	15
1161B-8R-1, 32-34	1.22	Basaltic breccia	Pervasive groundmass alteration	38
1162B-10R-1, 62-64	1.09	Basaltic breccia	Olivine completely altered, plagioclase Fe-stained	35
1163A-2R-1, 3-7	0.99	Moderately plagioclase olivine phyric basalt	Patchy groundmass alteration	30
1163A-2R-2, 10-15	1.02	Moderately plagioclase olivine phyric basalt	Alteration halos along veins	8
1163A-6R-1, 104-109	1.01	Aphyric basalt	Alteration halos along veins	7
1164A-3R-1, 8-11	1.01	Aphyric basalt	Slightly altered, concentric halos	22
1164B-4R-2, 55-60	0.92	Basaltic rubble	Slightly altered	18

Notes: Lithology from shipboard descriptions of intervals (Christie, Pedersen, Miller, et al., 2001). Alteration characteristics from billet examination. Secondary mineralogy from visual estimate.

Table T4. Correlation coefficients for geochemical, mineralogical, structural, and location data for altered sample. (Continued on next two pages.)

	Age (Ma)	Distance off axis (km)	Secondary mineralogy (modal%)	Major element oxides (wt%)											Ba (ppm)		
				SiO ₂	Al ₂ O ₃	Fe ₂ O ₃	MgO	CaO	Na ₂ O	K ₂ O	TiO ₂	P ₂ O ₅	MnO	Cr ₂ O ₃			
Age (Ma):	1.000																
Distance off axis (km):	1.000	1.000															
Secondary mineralogy (modal%):	0.376	0.370	1.000														
Major element oxides (wt%):																	
SiO ₂	-0.654	-0.654	-0.501	1.000													
Al ₂ O ₃	0.282	0.289	0.376	-0.410	1.000												
Fe ₂ O ₃	0.019	0.011	0.114	-0.013	-0.496	1.000											
MgO	-0.326	-0.314	-0.585	0.484	-0.244	-0.299	1.000										
CaO	0.266	0.262	0.305	-0.561	0.211	-0.383	-0.328	1.000									
Na ₂ O	-0.110	-0.111	0.065	0.182	0.177	0.145	-0.295	-0.489	1.000								
K ₂ O	0.420	0.416	0.209	-0.296	-0.040	0.176	-0.374	-0.096	0.047	1.000							
TiO ₂	-0.032	-0.041	0.021	0.084	-0.567	0.870	-0.307	-0.432	0.319	0.197	1.000						
P ₂ O ₅	0.170	0.172	0.208	-0.137	-0.296	0.653	-0.548	-0.158	0.395	0.266	0.734	1.000					
MnO	0.028	0.017	0.041	0.093	-0.429	0.773	-0.147	-0.290	0.052	0.025	0.705	0.420	1.000				
Cr ₂ O ₃	0.259	0.262	0.284	-0.260	0.471	-0.590	0.009	0.557	-0.293	-0.065	-0.685	-0.373	-0.586	1.000			
Trace elements (ppm):																	
Ba	-0.086	-0.091	-0.018	0.214	-0.060	-0.020	-0.122	-0.146	0.248	0.153	-0.014	0.139	0.006	-0.160	1.000		
Ni	0.237	0.247	-0.022	-0.162	0.208	-0.415	0.409	0.072	-0.322	0.003	-0.496	-0.365	-0.333	0.410	-0.153		
Sc	0.415	0.413	0.340	-0.357	-0.212	0.701	-0.522	-0.014	0.100	0.218	0.648	0.567	0.593	-0.197	-0.082		
Loss on ignition (LOI) (wt%)	0.298	0.292	0.330	-0.700	0.163	-0.205	-0.441	0.517	-0.086	0.414	-0.090	0.043	-0.269	0.077	-0.046		
Cu	0.428	0.423	0.276	-0.465	0.162	-0.053	-0.230	0.440	-0.316	0.071	-0.228	-0.131	-0.102	0.434	-0.026		
Zn	0.497	0.497	0.080	-0.277	-0.213	0.409	-0.329	-0.117	0.081	0.364	0.368	0.473	0.280	-0.077	0.054		
Ni	0.137	0.144	0.105	-0.158	0.364	-0.586	0.377	0.193	-0.249	-0.082	-0.634	-0.513	-0.427	0.474	-0.105		
Co	0.000	0.001	-0.120	0.090	-0.224	0.173	0.254	-0.069	-0.266	-0.175	0.098	-0.160	0.476	-0.153	-0.193		
Ga	0.124	0.120	0.116	0.073	-0.424	0.843	-0.367	-0.381	0.258	0.117	0.835	0.733	0.741	-0.524	0.064		
Hf	-0.060	-0.064	-0.031	0.154	-0.569	0.825	-0.262	-0.482	0.310	0.122	0.961	0.786	0.706	-0.726	0.081		
Nb	0.301	0.308	-0.245	-0.027	-0.048	0.085	0.102	-0.310	0.112	0.116	0.074	0.254	-0.011	-0.430	0.405		
Rb	0.320	0.311	0.027	-0.159	-0.204	0.370	-0.326	-0.142	0.077	0.789	0.355	0.280	0.332	-0.221	0.111		
Sr	-0.168	-0.172	-0.021	0.197	0.083	-0.415	-0.030	0.136	0.159	0.000	-0.287	-0.005	-0.297	0.050	0.359		
V	0.083	0.067	0.080	0.048	-0.522	0.899	-0.375	-0.355	0.240	0.133	0.937	0.710	0.724	-0.584	-0.031		
Zr	0.014	0.008	-0.088	0.172	-0.610	0.763	-0.194	-0.521	0.353	0.211	0.914	0.746	0.592	-0.726	0.089		
Y	-0.100	-0.107	-0.056	0.173	-0.596	0.859	-0.247	-0.489	0.322	0.119	0.975	0.741	0.682	-0.707	0.016		
La	-0.036	-0.041	-0.078	0.203	-0.415	0.564	-0.239	-0.462	0.428	0.197	0.730	0.713	0.489	-0.640	0.402		
Ce	0.177	0.178	-0.247	0.152	-0.438	0.394	-0.017	-0.445	0.256	0.248	0.464	0.442	0.292	-0.722	0.293		
Pr	-0.060	-0.065	-0.055	0.189	-0.552	0.753	-0.263	-0.487	0.366	0.165	0.919	0.809	0.652	-0.708	0.179		
Nd	0.005	0.000	-0.052	0.159	-0.544	0.786	-0.273	-0.479	0.336	0.163	0.933	0.806	0.688	-0.707	0.115		
Sm	0.018	0.013	-0.002	0.109	-0.536	0.811	-0.300	-0.449	0.310	0.140	0.951	0.810	0.711	-0.679	0.097		
Eu	0.236	0.231	0.176	-0.064	-0.475	0.821	-0.430	-0.321	0.283	0.286	0.929	0.860	0.711	-0.534	0.057		
Gd	-0.121	-0.126	-0.081	0.213	-0.573	0.845	-0.228	-0.521	0.289	0.065	0.961	0.756	0.729	-0.725	0.034		
Tb	-0.019	-0.023	-0.011	0.134	-0.538	0.867	-0.272	-0.502	0.285	0.124	0.974	0.771	0.755	-0.713	0.022		
Dy	-0.008	-0.012	0.004	0.107	-0.546	0.878	-0.303	-0.467	0.282	0.120	0.982	0.797	0.753	-0.685	0.006		
Ho	0.052	0.048	0.064	0.051	-0.541	0.883	-0.337	-0.426	0.268	0.166	0.982	0.811	0.766	-0.651	0.007		
Er	0.041	0.038	0.063	0.041	-0.527	0.885	-0.336	-0.434	0.273	0.162	0.985	0.807	0.761	-0.644	0.005		
Tm	-0.125	-0.129	-0.021	0.142	-0.562	0.884	-0.281	-0.475	0.261	0.078	0.979	0.747	0.758	-0.684	0.000		
Yb	-0.040	-0.044	-0.001	0.110	-0.551	0.882	-0.278	-0.478	0.255	0.107	0.981	0.759	0.768	-0.697	-0.016		
Lu	-0.054	-0.058	0.007	0.104	-0.545	0.887	-0.294	-0.471	0.263	0.116	0.979	0.764	0.772	-0.695	0.003		
Fractures and veins (N/m)	-0.323	-0.322	0.125	-0.400	0.057	-0.118	0.079	0.390	-0.442	-0.195	-0.304	-0.293	-0.185	0.212	-0.139		

Table T4 (continued).

	Trace elements (ppm)														
	Ni	Sc	LOI (wt%)	Cu	Zn	Ni	Co	Ga	Hf	Nb	Rb	Sr	V	Zr	Y
Age (Ma):															
Distance off axis (km):															
Secondary mineralogy (modal%):															
Major element oxide (wt%):															
SiO ₂															
Al ₂ O ₃															
Fe ₂ O ₃															
MgO															
CaO															
Na ₂ O															
K ₂ O															
TiO ₂															
P ₂ O ₅															
MnO															
Cr ₂ O ₃															
Trace elements (ppm):															
Ba															
Ni	1.000														
Sc	-0.287	1.000													
Loss on ignition (LOI) (wt%)	-0.014	-0.003	1.000												
Cu	0.107	0.398	0.180	1.000											
Zn	0.023	0.787	-0.026	0.471	1.000										
Ni	0.801	-0.492	0.210	0.025	-0.301	1.000									
Co	0.218	0.206	-0.197	0.107	0.073	0.117	1.000								
Ga	-0.426	0.679	-0.255	-0.082	0.521	-0.593	0.177	1.000							
Hf	-0.490	0.549	-0.153	-0.304	0.435	-0.609	0.088	0.824	1.000						
Nb	0.258	0.279	-0.245	0.045	0.615	-0.263	-0.159	0.440	0.560	1.000					
Rb	-0.173	0.314	0.247	0.064	0.346	-0.267	-0.041	0.241	0.234	0.077	1.000				
Sr	0.075	-0.439	0.040	-0.204	-0.237	0.150	-0.190	-0.132	-0.124	0.044	-0.132	1.000			
V	-0.476	0.737	-0.193	-0.085	0.466	-0.662	0.131	0.905	0.907	0.155	0.326	-0.321	1.000		
Zr	-0.357	0.521	-0.174	-0.273	0.484	-0.562	0.051	0.824	0.982	0.353	0.301	-0.082	0.866	1.000	
Y	-0.468	0.573	-0.188	-0.291	0.364	-0.637	0.121	0.845	0.968	0.146	0.274	-0.255	0.929	0.937	1.000
La	-0.418	0.293	-0.082	-0.344	0.314	-0.488	-0.121	0.667	0.812	0.824	0.300	0.264	0.689	0.849	0.741
Ce	-0.027	0.353	-0.251	-0.129	0.690	-0.306	-0.010	0.746	0.905	0.861	0.278	-0.008	0.481	0.687	0.524
Pr	-0.474	0.463	-0.129	-0.358	0.399	-0.597	-0.005	0.807	0.964	0.663	0.275	0.035	0.867	0.979	0.929
Nd	-0.486	0.496	-0.131	-0.360	0.407	-0.049	0.019	0.840	0.961	0.605	0.296	-0.053	0.898	0.972	0.947
Sm	-0.486	0.549	-0.112	-0.287	0.456	-0.620	0.062	0.851	0.963	0.554	0.263	-0.129	0.919	0.968	0.963
Eu	-0.400	0.715	-0.051	-0.135	0.623	-0.566	0.062	0.858	0.917	0.547	0.357	-0.155	0.915	0.921	0.899
Gd	-0.524	0.502	-0.214	-0.340	0.381	-0.646	0.090	0.839	0.968	0.476	0.219	-0.183	0.924	0.962	0.986
Tb	-0.490	0.581	-0.184	-0.291	0.442	-0.623	0.116	0.859	0.971	0.488	0.263	-0.219	0.944	0.964	0.985
Dy	-0.492	0.615	-0.156	-0.261	0.475	-0.637	0.112	0.868	0.971	0.487	0.267	-0.237	0.956	0.962	0.990
Ho	-0.468	0.675	-0.132	-0.204	0.543	-0.627	0.125	0.871	0.961	0.486	0.290	-0.255	0.959	0.955	0.978
Er	-0.456	0.669	-0.124	-0.214	0.536	-0.610	0.119	0.859	0.965	0.479	0.283	-0.272	0.956	0.954	0.981
Tm	-0.505	0.607	-0.190	-0.232	0.473	-0.654	0.141	0.822	0.953	-0.033	0.229	-0.283	0.937	0.938	0.988
Yb	-0.469	0.609	-0.159	-0.270	0.458	-0.622	0.153	0.849	0.967	0.439	0.246	-0.283	0.947	0.953	0.991
Lu	-0.478	0.616	-0.150	-0.258	0.471	-0.623	0.157	0.843	0.963	0.452	0.259	-0.263	0.942	0.952	0.989
Fractures and veins (N/m)	0.219	-0.079	0.179	0.208	-0.253	0.292	0.204	-0.273	-0.304	-0.140	-0.246	-0.045	-0.201	-0.313	-0.282

Table T4 (continued).

	Trace elements (ppm)														Fractures and veins (N/m)
	La	Ce	Pr	Nd	Sm	Eu	Gd	Tb	Dy	Ho	Er	Tm	Yb	Lu	
Age (Ma):															
Distance off axis (km):															
Secondary mineralogy (modal%):															
Major element oxide (wt%):															
SiO ₂															
Al ₂ O ₃															
Fe ₂ O ₃															
MgO															
CaO															
Na ₂ O															
K ₂ O															
TiO ₂															
P ₂ O ₅															
MnO															
Cr ₂ O ₃															
Trace elements (ppm):															
Ba															
Ni															
Sc															
Loss on ignition (LOI) (wt%)															
Cu															
Zn															
Ni															
Co															
Ga															
Hf															
Nb															
Rb															
Sr															
V															
Zr															
Y															
La	1.000														
Ce	0.941	1.000													
Pr	0.916	0.961	1.000												
Nd	0.877	0.948	0.985	1.000											
Sm	0.829	0.910	0.963	0.977	1.000										
Eu	0.749	0.832	0.906	0.917	0.929	1.000									
Gd	0.788	0.881	0.951	0.965	0.970	0.887	1.000								
Tb	0.769	0.874	0.943	0.965	0.970	0.922	0.985	1.000							
Dy	0.758	0.859	0.939	0.959	0.972	0.936	0.983	0.989	1.000						
Ho	0.733	0.836	0.923	0.942	0.965	0.958	0.960	0.980	0.989	1.000					
Er	0.730	0.831	0.922	0.940	0.964	0.954	0.962	0.980	0.990	0.995	1.000				
Tm	0.696	0.796	0.901	0.912	0.937	0.887	0.968	0.970	0.974	0.970	0.975	1.000			
Yb	0.719	0.833	0.918	0.940	0.962	0.914	0.980	0.986	0.990	0.983	0.989	0.985	1.000		
Lu	0.729	0.831	0.919	0.935	0.958	0.915	0.975	0.980	0.987	0.982	0.987	0.988	0.993	1.000	
Fractures and veins (N/m)	-0.363	-0.208	-0.331	0.235	-0.357	-0.317	-0.327	-0.304	-0.299	-0.295	-0.281	-0.266	-0.274	-0.265	1.000